JOURNAL OF SOLID STATE CHEMISTRY 21, 303–324 (1977)

Rare-Earth Orthovanadates: Covalency, Chemical Bonding, and Optical Spectra*

V. A. GUBANOV,† D. E. ELLIS,‡ AND A. A. FOTIEV†

†*Institute of Chemistry, Ural Science Center, Academy of Sciences, Sverdlovsk, GSP-169, USSR and* ‡*Departments of Physics and Chemistry, and Materials Research Center Northwestern University, Evanston, Illinois 60201*

Received February 1, 1977

Investigations of electronic structure and optical spectra were made for yttrium orthovanadate, and for rare earth orthovanadates RVO_4, where R = Ce, Nd, Eu, Tb, Dy, Gd, and Yb. The Hartree–Fock–Slater model was used in conjunction with a numerical discrete variational method to calculate energy levels and wavefunctions for molecular clusters $(VO_4)^{3-}$ and $(RO_8)^{13-}$ found in the orthovanadate crystal lattice. Analysis of the MO charge and spin densities reveals a significant involvement of rare earth 4*f* orbitals in chemical bonding, through hybridization of R–5*p* and mixing with O–2*p* atomic orbitals. The MO energy level diagrams provide a satisfactory semiquantitative interpretation of the experimental excitation, reflection, and luminescence spectra. Energy transfer from the vanadate ion to the rare-earth ion is understood in terms of covalent mixing between metal and shared O–2*p* orbitals for neighboring $(VO_4)^{3-}$ and $(RO_8)^{13-}$ clusters. The relative luminescent efficiency of some rare-earth elements is explained on the basis of the calculated energy level diagrams.

1. Introduction

Rare-earth vanadates with the formula RVO_4 are of considerable interest from several points of view. First, they reveal luminescent properties, which take place without activation, caused by electron transitions in the tetrahedral vanadate ion. After the introduction of activators (a rare-earth ion) the orthovanadates become very efficient phosphors. These materials are used in quantum optics and as a coating in luminescent lamps. The europium-activated yttrium orthovanadate is a red phosphor widely used in color television tubes (*1*). With activation by neodymium ions, laser materials for the ir region have been obtained (*2*). The introduction of erbium and Tm ions into the orthovanadate crystal lattice leads to laser materials for the visible part of the optical spectrum (*3*, *4*). While terbium orthovanadate does not show any luminescence, the terbium ions are, however, quite active in other matrices, such as RPO_4, where activation of Tb^{3+} results in intense green luminescence (*5*). Actually, in the orthovanadate lattice, the terbium ion appears to be an effective quencher of luminescence, rather than an activator (*6*). Similarly, Ce^{3+} ions in phosphates show an intense luminescence in the uv region, but fluoresce only weakly in the ir region when added to vanadates.

Optical properties of the orthovanadates have been studied in a large number of experimental works (see Ref. (*1*, Bibliography)), but still many questions connected with the nature of optical characteristics and luminescence, with the mechanisms of energy transfer from

* Research supported in part by the Air Force Office of Scientific Research, under Grant 71-2021G.

ISSN 0022-4596

the excited vanadate ions to the emitting rare-earth ions, or the optical activity of some rare-earths in the vanadate crystal lattice and its absence for others, as well as the peculiarities of energy level diagrams for the compounds, are not clear enough.

The rare-earth orthovanadates are the most interesting and convenient objects for the study of chemical bonding effects of rare-earth elements, i.e., the influence of different populations in the $4f$ shell on the energy levels and charge distribution—especially covalency effects and the participation of $4f$ orbitals in chemical bonding. In the present paper, the electronic structure of rare-earth orthovanadates is studied, using the $X\alpha$ Hartree–Fock–Slater model implemented by the discrete variational method (*8*, *9*). Calculations have been carried out for VO_4^{3-} and RO_8^{13-} clusters characteristic of the orthovanadate crystal lattice. Energy level diagrams, charge distributions, and spin densities have been obtained in a spin-unrestricted formalism. Covalency effects and the role of the $4f$ electrons in chemical bonding of the orthovanadates are quantitatively discussed. Theoretical results are compared with the experimental excitation, reflection, and luminescence spectra of these compounds.

2. Geometrical Structure of Clusters in the Rare-Earth Vanadates

Two types of crystal lattice are characteristic of the rare-earth orthovanadates, the most common being the zircon structure with the symmetry of the D_{4h}^{19} space group (*10–13*). The second type includes $LaVO_4$, which possesses a monoclinic crystal lattice of monacyte type, along with several other rare-earth vanadates (*14*, *15*). In the present paper, we study only those compounds which are isostructural to YVO_4, with the zircon structure.

The yttrium orthovanadate crystal lattice has been studied in detail (*16*). Every vanadium atom is surrounded by four oxygen atoms, which form a slightly distorted tetrahedral environment with a common V–O bond length of 1.706 Å. The yttrium atom is coordinated to four nearest oxygens with the Y–O(1) bond length of 2.299 Å and a second set of four oxygens with bond length Y–O(2) of 2.443 Å. The symmetry of the YO_8 cluster is D_{2d} (see Fig. 1). This type of crystal lattice is unaltered when yttrium is replaced by various rare-earth ions. The lattice constants for rare-earth (RE) vanadates are given in (*10*, *11*) and the detailed structure for some of them is described in (*11*, *12*). Although the geometry of the vanadate ion does not change, the bond lengths do vary slightly: for $NdVO_4$ the V–O bond length is 1.721 Å, and Nd–O(1) and Nd–O(2) lengths are 2.398, and 2.492 Å, respectively (*11*). In $DyVO_4$ the corresponding values are 1.722, 2.282, and 2.442 Å, for $TbVO_4$ they are 1.721, 2.311, and 2.451 Å, and in ytterbium orthovanadate, they are equal to 1.711, 2.251, and 2.442 Å (*12*).

The calculations of RO_8^{13-} clusters presented here have been carried out for the actual D_{2d} structure of their respective orthovanadate lattices. The VO_4^{3-} cluster was treated for two geometrical structures, that of the ideal tetrahedron and the geometry of the vanadate ion in YVO_4.

According to the experimental optical properties all orthovanadates RVO_4 are usually divided into two groups (*7*). The first group includes those vanadates which do not show any additional bands connected with the RE ion in the near uv and visible region of

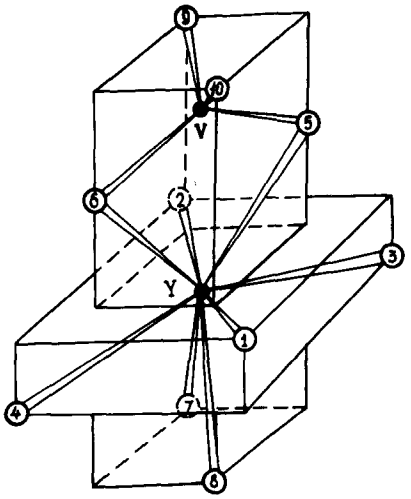

FIG. 1. Crystal structure of yttrium orthovanadate.

absorption and emission spectra. These include the orthovanadates of yttrium, lanthanum, cerium, gadolinium, and lutecium. The second group consists of compounds whose spectra reveal peaks produced by RE ions, which are of the greatest interest as optical materials.

3. Method of Calculation

Using the spin-polarized $X\alpha$ Hartree–Fock–Slater model, we have carried out electronic structure calculations for clusters belonging to orthovanadates of the first group $-RVO_4$, where $R = Y$, Ce, Gd and a number of examples from the second group $-LVO_4$, where $L = Nd$, Eu, Tb, Yb. The Hartree–Fock–Slater (HFS) equations were solved by a discrete variational method with numerical atomic orbitals as a basis set (*9*). The one-electron Hamiltonian based on Slater's statistical exchange approximation (*17*) is

$$h_\sigma = -\tfrac{1}{2}\nabla^2 + V_{\text{Coul}}(\mathbf{r}) + V_{\text{ex},\sigma}(\mathbf{r}), \qquad (1)$$

where V_{Coul} the Coulomb potential:

$$V_{\text{Coul}} = -\sum_\nu \frac{Z_\nu}{|\mathbf{r} - \mathbf{R}_\nu|} + \int d^3 \frac{\mathbf{r}'\,\rho(\mathbf{r}')}{|\mathbf{r} - \mathbf{r}'|} \qquad (2)$$

is defined through the total density of electrons of both spins

$$\rho(\mathbf{r}) = \rho_\uparrow(\mathbf{r}) + \rho_\downarrow(\mathbf{r}). \qquad (3)$$

$V_{\text{ex},\sigma}$ is the local exchange potential for an electron with spin σ ($\sigma = \uparrow$ or $\downarrow$) given in Hartree atomic units as

$$V_{\text{ex},\sigma}^{(\mathbf{r})} = -3\alpha\{(3/4\pi)\,\rho_\sigma(\mathbf{r})\}^{1/3}, \qquad (4)$$

where the exchange constant α is generally chosen either on empirical grounds or to satisfy some free atom criterion, $\frac{2}{3} \leqslant \alpha \leqslant 1$. Variational solutions of the Schrödinger equation

$$h_\sigma \psi_n = \varepsilon_i^\sigma \psi_n^\sigma, \qquad (5)$$

were obtained by expanding the eigenfunctions of spin σ, ψ_n^σ, in a linear combination of symmetrized atomic orbitals. The required Hamiltonian and overlap matrix elements were calculated by numerical integration using a discrete set of sampling points generated by a weighted diophantine procedure (*18*). Approximate convergence of 0.1 eV was observed for valence levels with 2000 points. The atomic basis functions were taken to be numerical solutions of the Hartree–Fock–Slater model, with exchange parameters α_i recommended by Schwarz (*20*, *21*). The variational basis consisted of all core and valence levels of the free atoms; i.e., oxygen $1s$, $2s$, $2p$, vanadium $1s\cdots3d$, $4s$, $4p$, and rare-earth $1s\cdots4f$, $5d$, $6s$, $6p$. For the cluster calculations, the α value of Eq. 4 was taken to be the average of the atomic values. The potential was constructed by superposition of free-atom spin densities, *without* introducing the "muffin-tin" approximation; the calculations were not iterated to self-consistency.

4. Cluster Molecular Orbitals: Covalency Effects in RVO_4

Valence orbital energies for the $(VO_4)^{3-}$ and $(YO_8)^{13-}$ clusters are given in Fig. 2. The MO diagram obtained for the vanadate ion in the present calculations agrees quite reasonably with the results we obtained earlier by the scattered-wave $X\alpha$ method (*22*). The separation of groups of orbitals with dominant contributions of O–$2s$, $2p$, and V–$3d$ orbitals is close to the data of (*22*); however, the ordering of levels within the $2p$ "band" is somewhat different. Due to the covalency effects, there are significant contributions of vanadium $3d$, $4s$, and $4p$ states in eigenfunctions of the "oxygen $2s$, $2p$" bands. Similarly, the low-lying vacant levels (especially $2e$, $7t_2$ with predominant V–$3d$ character), contain significant contributions from O–$2p$ states. The $2e$ level has ~40% oxygen character; the $7t_2$ level correspondingly has ~35% O–$2p$, and ~10% V–$4p$ character as allowed by the tetrahedral geometry. The $7t_2$ level also includes a small O–$2s$ admixture.

Comparatively small distortions of the $(VO_4)^{3-}$ cluster as found in the rare-earth orthovanadate (ROV) lattice result in rather small splittings of the MO energy levels and in small changes of orbital ordering and composition. Therefore, those differences reported for the vanadate-ion structure in the ROV

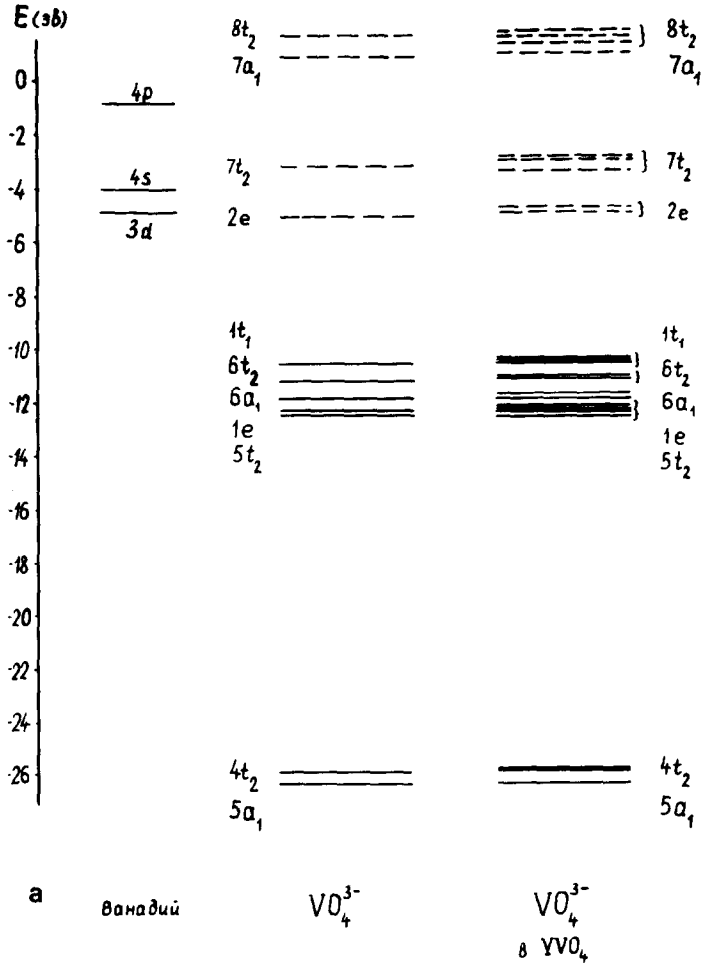

FIG. 2. Energy levels of clusters: (a) $(VO_4)^{3-}$ in perfect tetrahedral symmetry, and with D_{2h} symmetry of YVO_4 (b) $(YO_8)^{13-}$ in D_{2d} distorted octahedral symmetry. (c) $(EuO_8)^{13-}$ in D_{2d} symmetry.

series (*12*) do not lead in practice to significant MO level shifts.

Energy levels of the distorted octahedral $(YO_8)^{13-}$ cluster are shown in Fig. 2b. MO levels $8a_1 \cdots 8e$ are composed mainly of O–2*s* orbitals with a small admixture of yttrium 4*d*, 5*s*, 5*p* orbitals. MO's predominantly of oxygen 2*p* character (but containing large metal covalent contributions) are found about 13 eV higher. This interval is close to the difference in ionization potentials for atomic O–2*s* and 2*p* electrons. Among the higher "antibonding" band of vacant orbitals, $4b_1$, $14a_1$, $13b_2$, and 16*e* MO's have strong yttrium 4*d* character; 14*e* and 16*e* arise from metal 5*p*, and $15a_1$ from Y–5*s*. Of course, these antibonding levels include essential covalent contributions from oxygen wavefunctions. We see, in general, that the relatively low D_{2d} symmetry of the $(YO_8)^{13-}$ cluster leads to strong splittings of the MO levels, compared to results for an undistorted octahedral structure. Further, we find a considerable mixing of oxygen 2*s*, 2*p* with metal 4*d*, 5*s*, 5*p* states which then form bonding and antibonding bands separated by 6.5 eV (see Table I). In the table, one can also see that core orbitals are reproduced, with energies near to that of the parent atom.

In Figs. 2–5 we present the calculated level structures for $(RO_8)^{13-}$ clusters, where R = Eu, Ce, Nd, Gd, Tb, Dy, and Yb. As a full presen-

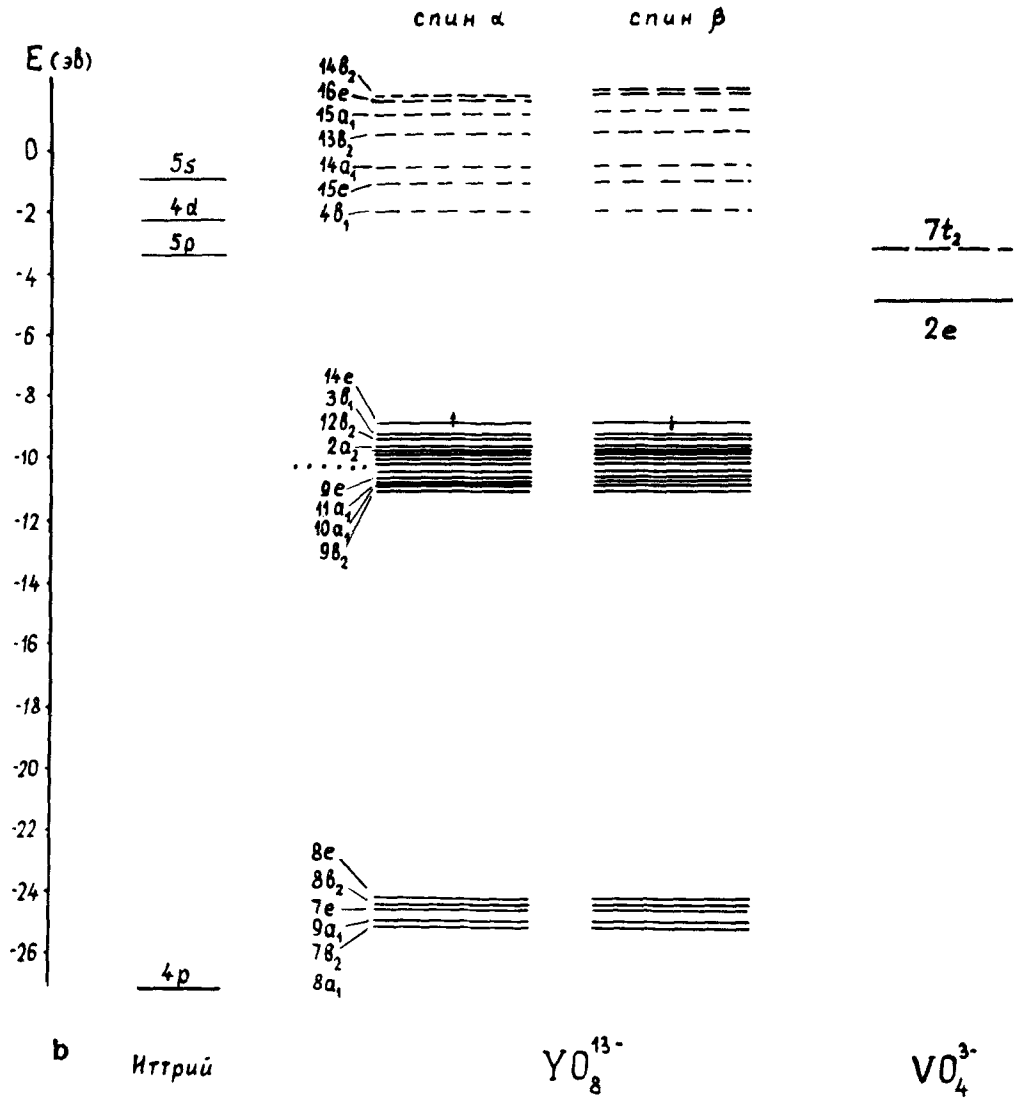

FIG. 2—*Continued*

tation of the results would be too lengthy, we discuss here in detail only the most interesting representative of this series, europium (Fig. 2c). Energy levels for the $(EuO_8)^{13-}$ cluster are presented in Table II. Molecular orbital energies ($8e\cdots 10e$) in the interval −20 to −26 eV are predominantly O–2*s* mixed with Eu–5*p* character. This mixing leads to a small but noticeable spin-splitting of the O–2*s* band. The 9*e* MO consists entirely of O–2*s* character, while $9b_2$ shows a small admixture of Eu–5*p*, 5*d*. The 8*e*, 10*e*, $8b_2$, $10b_2$ levels show strong Eu–5*p* character, up to 60% in the 10*e* orbital; it is interesting that small amounts of Eu–4*f* character appear in the b_2 levels, as allowed by symmetry. Similarly, the a_1 levels of this group also show small covalent contributions from metal 4*f*, 5*s*, and 5*d* states.

The spin-polarized valence band covers the interval −8 to −12 eV (see Fig. 2c), the occupied states terminating with $18e\uparrow$ and $16e\downarrow$. The densely spaced levels are predominantly O–2*p* in character, but with strong $4f\uparrow$ metal components, as expected from the assumed

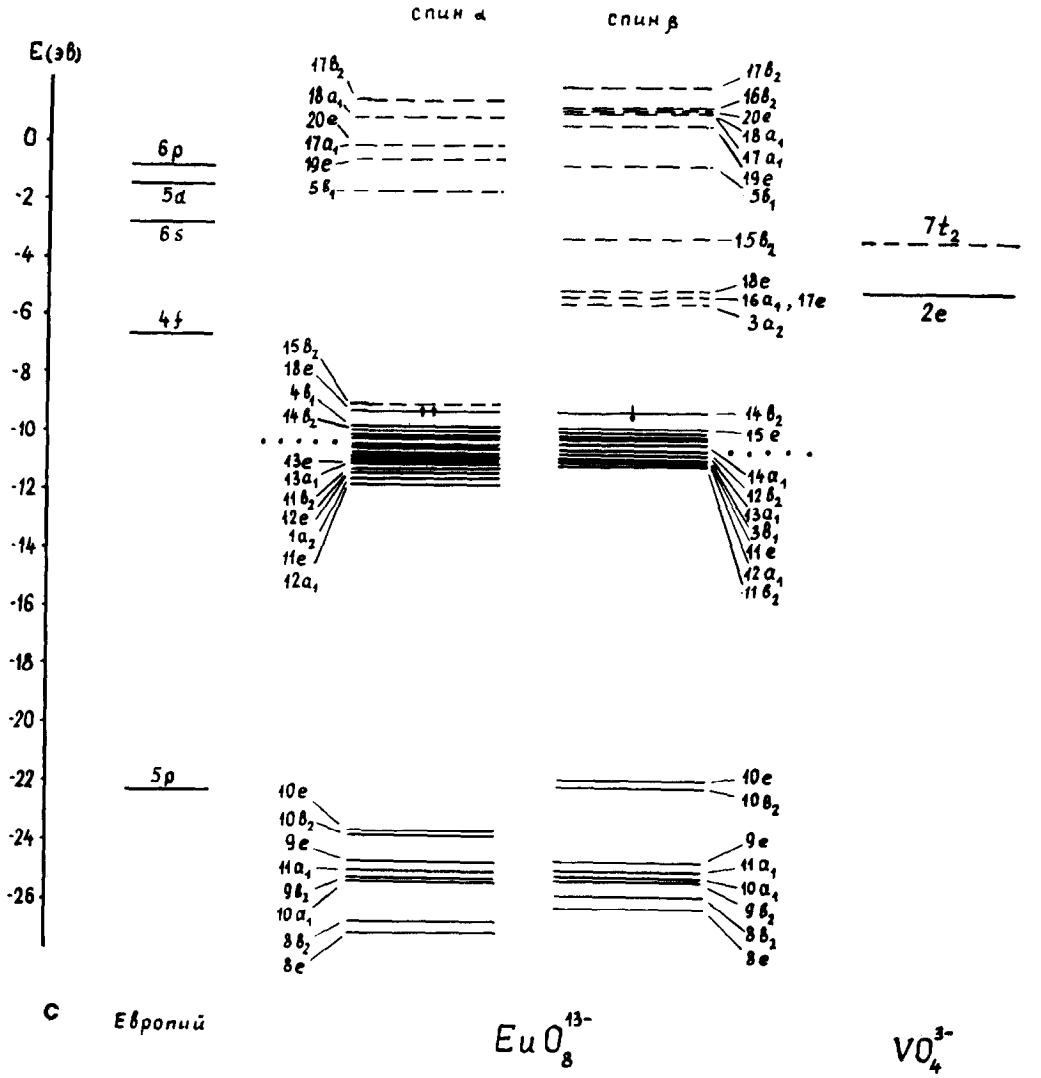

FIG. 2—*Continued*

$(4f\uparrow)^7$ configuration of the input atomic states. Additional covalent metal contributions are noted: for example, the $3b_1\uparrow$ and $11b_2\uparrow$ MO's contain ~15% Eu-5*d* character. Hybridization of the oxygen *p*-band also extends to Eu-4*f* orbitals, which, for example, contribute ~15% to the $12b_2\uparrow$ level with noticeable metal *p* contributions as well. Similar hybridization is observed for levels of *e* symmetry (16*e*, 17*e*) and $a_1\uparrow(15a_1)$. The energy overlap of $4f\uparrow$ and O-2*p* levels leads to a spin ↑ valence band somewhat broader than that for spin ↓, but with approximately the same center. The bottom of the spin ↑ band consisting of the six states $12a_1$, 11*e*, $1a_2$, 12*e*, is predominantly of $4f$ type, although up to 30% oxygen admixture is found. The seventh $4f$ level, $15b_2$, is pushed up by ~2.5 eV and forms the first *unoccupied* spin ↑ state.

Due to spin-polarization effects, the spin ↓ group of $4f$ levels is separated by nearly 6 eV from the corresponding $4f\uparrow$ set of levels and are thus completely unoccupied. The spin splitting found here is quite consistent with

TABLE I

MOLECULAR ORBITAL ENERGIES FOR THE $(YO_8)^{13-}$ CLUSTER

Orbital	MO energy (Ry)	Corresponding atomic Level (Ry)	Orbital	Energy (Ry)
$1a_1$ (Y 1*s*)	−1214.01[a]	−1212.42	$8e$	−1.79
$2a_1$ (2*s*)	−164.49	−163.83	$9b_2$	−0.817
$1e$ (2*p*)	−150.55	−149.84	$10a_1$	−0.814
$1b_2$			$11a_1$	−0.807
$2e$ (O 1*s*)	−37.85	−37.83		
$3a_1$			$9e$	−0.800
$2b_2$			$2b_1$	−0.792
$3e$			$10b_2$	−0.769
$4a_1$			$10e$	−0.761
$3b_2$			$11b_2$	−0.756
$5a_1$ (Y 3*s*)	−26.29	−26.02	$12a_1$	−0.750
$4e$ (3*p*)	−21.11	−20.83	$11e$	−0.733
$4b_2$			$1a_2$	−0.726
$5e$ (3*d*)	−11.64	−11.36	$12e$	−0.715
$1b_1$			$13e$	−0.700
$5b_2$			$13a_1$	−0.700
$6a_1$			$2a_2$	−0.700
$7a_1$ (4*s*)	−3.47	−3.35	$12b_2$	−0.695
$6e$ (4*p*)	−2.16	−2.00	$3b_1$	−0.692
$6b_2$ (4*p*)	−2.15		$14e$	−0.657[b]
$8a_1$	−1.84		$4b_1$	−0.185
$7b_2$	−1.83		$15e$	−0.109
$9a_1$	−1.81		$14a_1$	−0.075
$7e$	−1.80		$13b_2$	+0.014
$8b_2$	−1.79		$15a_1$	+0.050
			$16e$	+0.104
			$14b_2$	+0.126

[a] Uncertainty of ~2 Ry in core level for 2000 integration points; uncertainty in valence levels ~0.1 eV.
[b] Last occupied level.

results found for the $(EuO_6)^{10-}$ system (*23*). The crystal field splittings of the $4f\downarrow$ levels ($3a_2 \cdots 15b_2$) are clearly evident in Fig. 2*c*; the V–3*d* ($7t_{2g}$, $2e$) levels of the vanadate ion are indicated at the extreme right of the figure for future reference. The uppermost $(EuO_8)^{13-}$ levels are combinations of metal 5*d* ($5b_1$, $17b_2$, $19e$, $17a_1$), 6*s* ($18a_1$), and 6*p* ($16b_2$, $20e$) character with significant ligand orbital hybridization. Due to strong mixing of Eu↑ and ligand levels found here, we show by quantitative population analysis that the net distribution of the charge is not consistent with the traditional ionic picture. Moreover, it is obvious that the strong hybridization of cluster wavefunctions leads to selection rules for excitation processes quite different from those of a purely ionic model.

As seen from Table II, the metal core orbitals show significant exchange splittings, increasing from about 0.2 Ry for the 3*d* levels to 0.5 Ry for 4*s*, 4*p*, and 4*d* levels. The experimental value for the splitting of Eu–4*s* states is reported as 0.52 Ry (*24*). Since the present calculations are nonrelativistic, spin-orbit effects have not been included, and we are unable to describe the complicated structure of the 4*d* levels found in Ref. (*25*). Indeed, an adequate description of such structures may go beyond one-electron models. From the present calculations, one can get an estimate of the rather small crystal field splittings of inner levels.

Similar extensive calculations were made for the MO structure and level splittings for the remaining $(RO_8)^{13-}$ clusters with resulting level schemes shown in Figs. 3–5. These diagrams allow a discussion of significant changes in the rare-earth orthovanadate level structure due primarily to different degrees of occupancy of the rare-earth 4*f* shell. One can immediately see that, with the exception of the group of levels of predominant 4*f* type, the relative positions of the cluster MO levels do not change very much. Nevertheless, some interesting trends in the substructure of the valence bands can be found.

Let us first consider the lowest valence band consisting of oxygen 2*s* and metal 5*p* states. Orbitals which contain no 5*p* admixture ($9b_2$, $10a_1$, $11a_1$, $9e$) remain constant in energy, with negligible spin splitting. The systematic lowering of the atomic 5*p* level in the series Ce, Nd, Eu, Gd, Tb, Dy, Yb causes a progressive mixing with symmetry-allowed O–2*s* MO's with resulting level shifts and polarization changes. Thus, in the $(CeO_8)^{13-}$ cluster (Fig. 3a), the 5*p* levels ($10b_2$, $10e$) are found nearly 4 eV above nearly pure O–2*s* levels and direct polarization by the incomplete 4*f* shell is very small. Hybridization of 5*p* and O–2*s* states

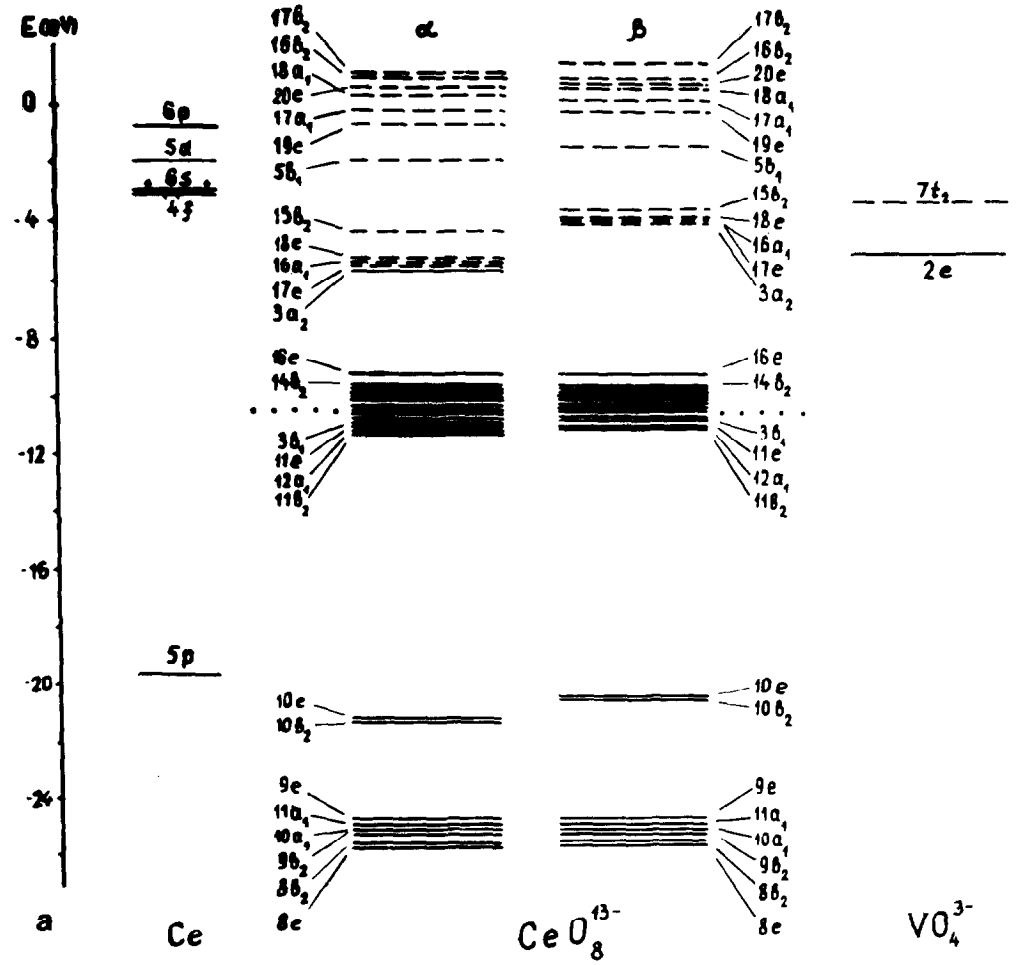

FIG. 3. Valence molecular orbital energies for the ground state of (a) $(CeO_8)^{13-}$, (b) $(NdO_8)^{13-}$ clusters.

begins to be significant for the neodymium cluster (Fig. 3b). Coinciding with maximum polarization of the $4f$ shell for Eu and Gd, we find that the spin ↑ $5p$ and O–$2s$ bands have essentially merged while spin ↓ levels remain largely distinct. Proceeding to the heavier members of the series, the $5p$ level moves progressively lower in energy and the polarization decreases, so that the $(YbO_8)^{13-}$ levels (Fig. 5b) show an inverted structure compared to the cerium case. We should remark that the almost exact agreement between spin ↑ and spin ↓ levels found for the $(YbO_8)^{13-}$ cluster is an artifact of the spin-restricted atomic orbitals used in constructing the $(4f\uparrow)^7\,(4f\downarrow)^6$ polarized configuration. Self-consistent iterations on the molecular potential introduce small exchange splittings without affecting our conclusions.

The most striking changes in the cluster energy level diagrams are connected with orbitals predominantly of $4f$ type. The interaction of these levels with the oxygen $2p$ band is similar to, but more dramatic than, that discussed for the O–$2s$, metal $5p$ states. For the cerium orthovanadate we find a separation of ~3.5 eV between the occupied $4f\uparrow$ ($3a_2$) level and the ligand band; for neodymium, the three occupied $4f\uparrow$ ($3a_2$, $17e$) states have moved to within ~1 eV of the ligand band and hybridization with the O–$2p$ atomic orbitals becomes noticeable. (For a quantitative measure of the total $4f$ orbital occupancy, it is necessary to consider the Mulliken population analysis

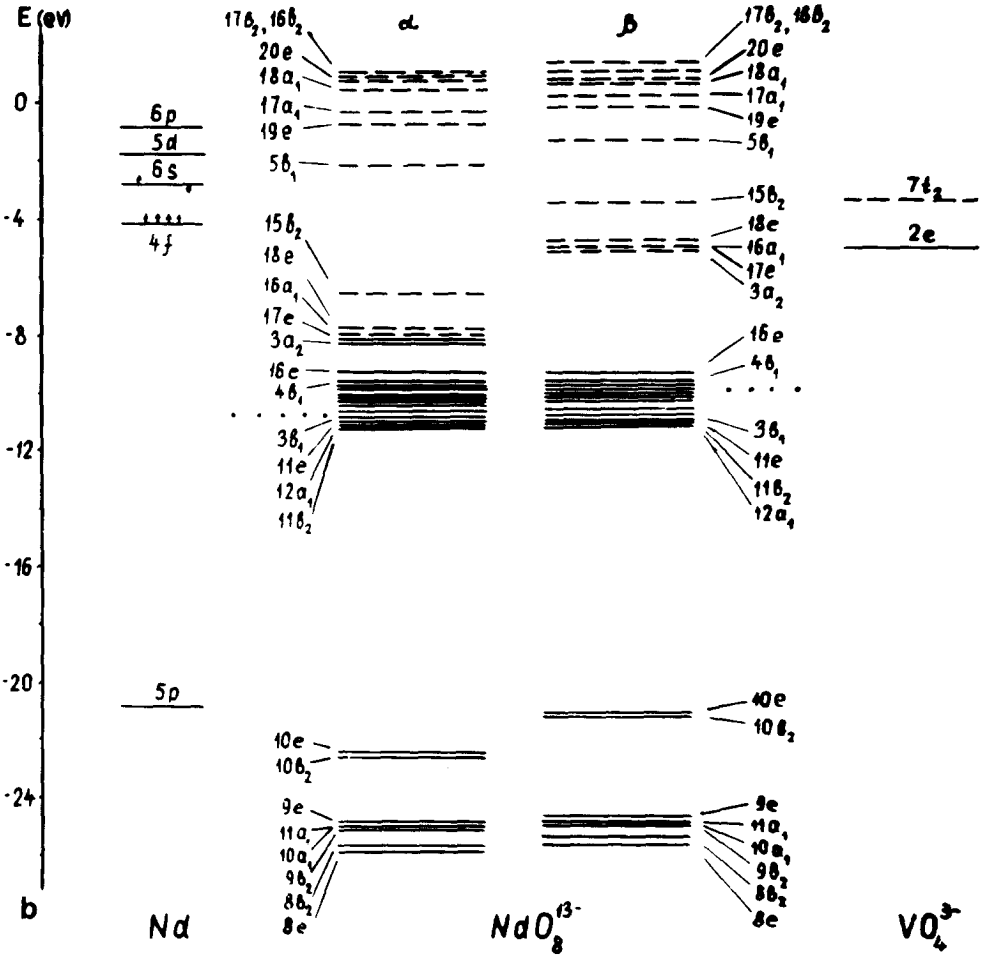

FIG. 3—*Continued*

given in Table III; these results are discussed in a following section.) The $4f\uparrow$–$4f\downarrow$ exchange splitting has simultaneously increased from about 1.5 eV (Ce) to 3 eV (Nd). Sizable crystal field splittings are noticeable; e.g., the $15b_2$ level in Nd is separated by ~1.5 eV from the lower members of the $4f$ group. The specific combination of spin splitting and crystal field splittings found for a particular *R*OV is critical for establishing the conditions for resonant energy transfer from vanadate ion to rare-earth ion, as we discuss below.

The trends in $4f$ level shifts and $4f$ mixing with O–$2p$ are now clear. For europium, there is considerable overlap between $4f\uparrow$ and ligand levels; for gadolinium, the two bands have completely merged and spin polarization effects are quite large. In the case of $(GdO_8)^{13-}$ the $4f\uparrow$ shell is completely filled while $4f\downarrow$ is empty with a predicted gap in the one-electron excitation spectrum of ~3 eV. These trends are continued with increasing rare-earth atomic number, as the $4f\uparrow$ character moves continually downward through the valence band and the $4f\downarrow$ levels become successively occupied and merge with the spin $\downarrow$ ligand band. In the limiting case of $(YbO_8)^{13-}$ the lowest states of either $\uparrow$ or $\downarrow$ valence bands are essentially of $4f$ character.

In contrast to the assumptions of "classical" crystal field theory which is still often used for the interpretation of level structure in RE compounds, we find the following effects to be most important:

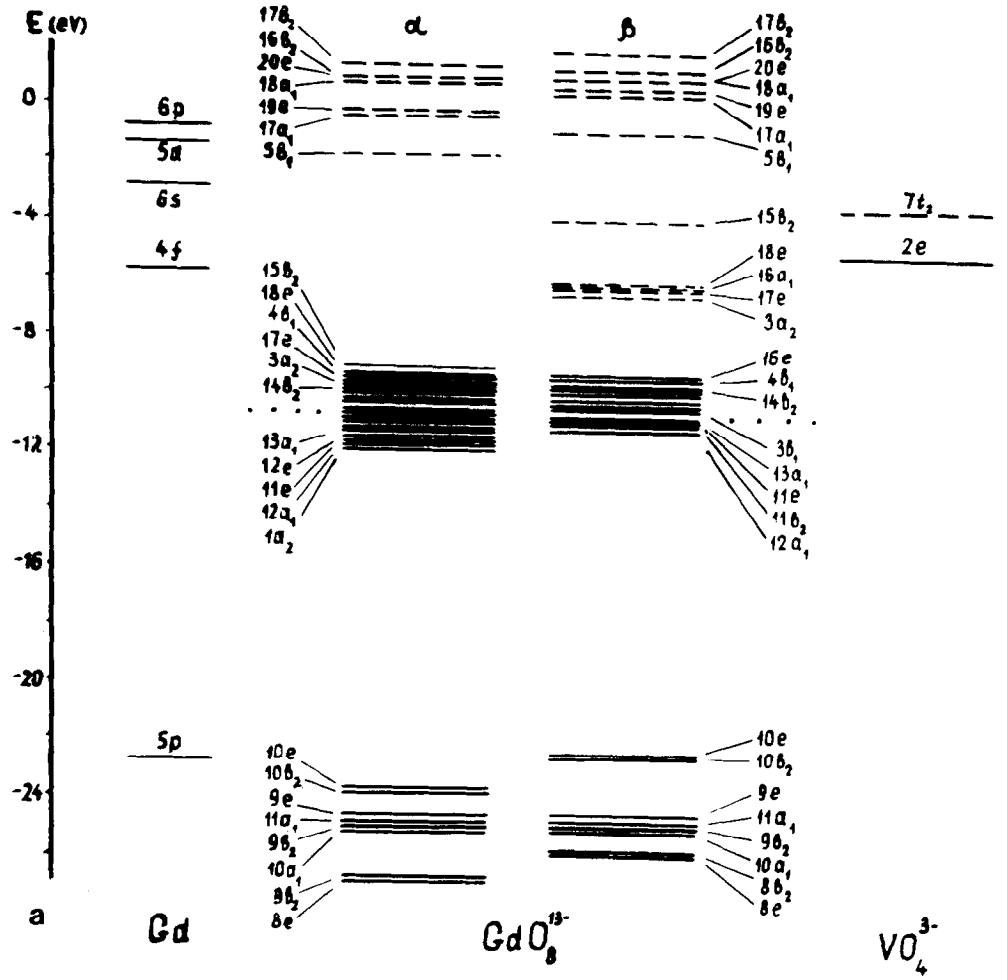

FIG. 4. Valence molecular orbital energies for ground state of (a) $(GdO_8)^{13-}$, (b) $(TbO_8)^{13-}$ clusters.

1. Spin polarization of the $4f$ levels of the cluster is typically large compared with crystal field effects, increasing rapidly to the middle of the rare-earth period and decreasing thereafter.

2. The crystal field splitting for $4f$ levels of a given spin increases rapidly across the series, being primarily due to hybridization as the atomic $4f$ level moves to lower energy and merges with the ligand $2p$ band.

The latter point implies, of course, that $4f$ orbitals are active participants in chemical bonding of these compounds. This view receives experimental confirmation on studying isotope chemical shifts in ^{51}V NMR spectra of the vanadates (*26*). This work shows significant unpaired spin density at the vanadium site, which must result from covalent spin transfer from the rare-earth through the shared oxygen atoms (see also Ref. (*27*)).

Specific information about the role of covalency for rare-earth elements in these compounds can be obtained from Table III where the populations of atomic orbitals, electronic configurations, and spin densities for the metal atoms are given. Although Mulliken populations are basis set dependent, relative comparisons are certainly meaningful. Due to covalent contributions, the population of $4f$ atomic orbitals grows essentially in accordance with accepted models (for example, $4f^1$ for Ce, $4f^6$ for Eu, etc.). Approximately

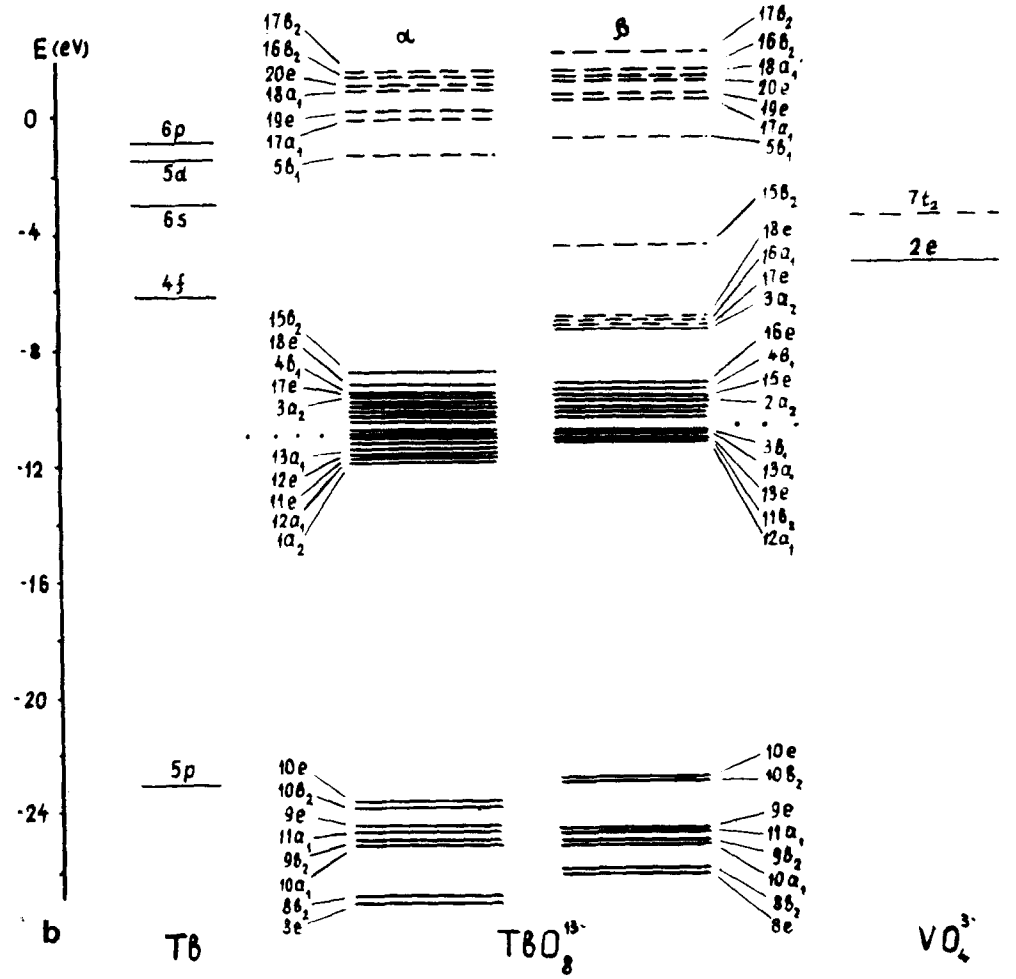

FIG. 4—*Continued*

one 5*d* electron is occupied, with small contributions also due to 6*s* and 6*p* atomic orbitals. It is especially interesting to note the occupancy of $4f\downarrow$ states; for Ce to Gd these contributions are purely due to covalent mixing.

The net atomic configurations derived from the data of Table III are very different from those of classical crystal field theory. Taking Eu as an example, the purely ionic configuration $4f^6 5d^0 6s^0 p^0$ is modified by covalency effects to $4f^{6.23} 5d^{1.0} 6s^{0.04} 6p^{0.05}$. The effective ion charge is thus reduced considerably from the +3 value of the ionic model, in a manner similar to that observed in most MO calculations on transition metal compounds.

A crude picture of spin distribution in the orthovanadates can be found from the net spin populations (Table III). Again, due to covalent effects, spin configurations are different from assumptions of the ionic model, but to a lesser degree than for charge configurations. Spin densities in the 4*f* orbitals, of course, increase from Ce to Gd and decrease thereafter; deviations from ionic values do not exceed 0.2 electron. Similar tendencies are observed for polarization of the 5*d* shell, which reaches a maximum value of 0.07 to 0.08 for Eu and Gd. Polarization of 5*s*, 5*p*, 6*s*, and 6*p* shells is seen to be one order of magnitude smaller still, the inner shells showing a *negative* polarization.

The effective configuration of the yttrium in $(YO_8)^{13-}$ given at the bottom of the table con-

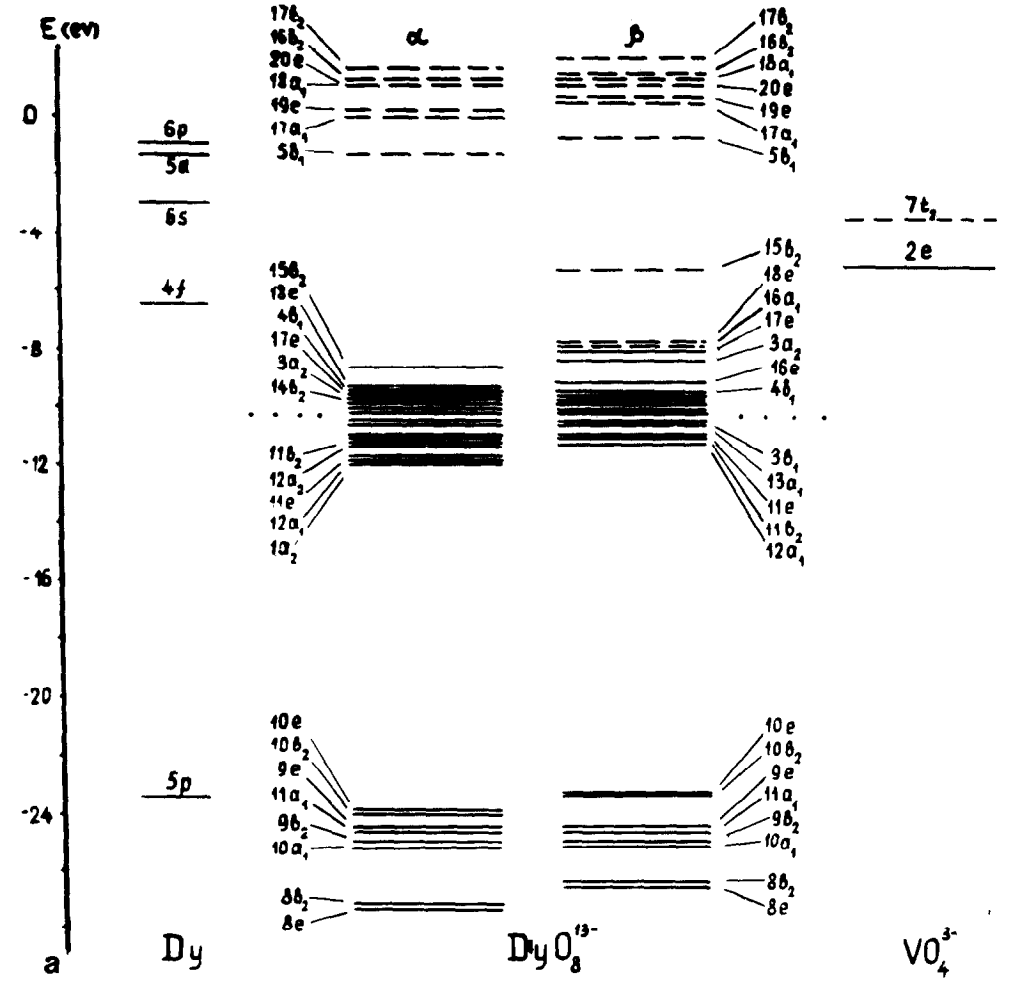

FIG. 5. Valence molecular orbital energies for ground state of (a) $(DyO_8)^{13-}$, (b) $(YbO_8)^{13-}$ clusters.

firms ideas about the similarity of the charge state of Y and the rare-earths in these compounds.

5. Electronic Spectra and Energy Levels of YVO_4 and YVO_4–Eu

The cluster energy level diagrams given in Figs. 2–5 can be used for the interpretation of the electronic optical spectra of the vanadates under study. The values obtained are *one-electron* eigenvalues of an approximate ground state Hamiltonian, and give only average energies of multiplets. Energy differences obtained from the eigenvalues do not permit a description of multiplet structure of the separate terms (*17*, *28*). However, for rare-earth ions and the compounds under consideration, the energy distances between terms are essentially larger than multiplet splittings. Another question concerns the omission of possibly significant final-state relaxation effects in our "frozen orbital" description of the excitation process. Calculation of these effects by Slater's transition state procedure has shown that for valence excitations of many systems, resulting level shifts are either uniform or small. Although more sophisticated calculations would be very interesting, we find the present level scheme very useful in understanding the optical characteristics of rare-earth elements in the vanadates.

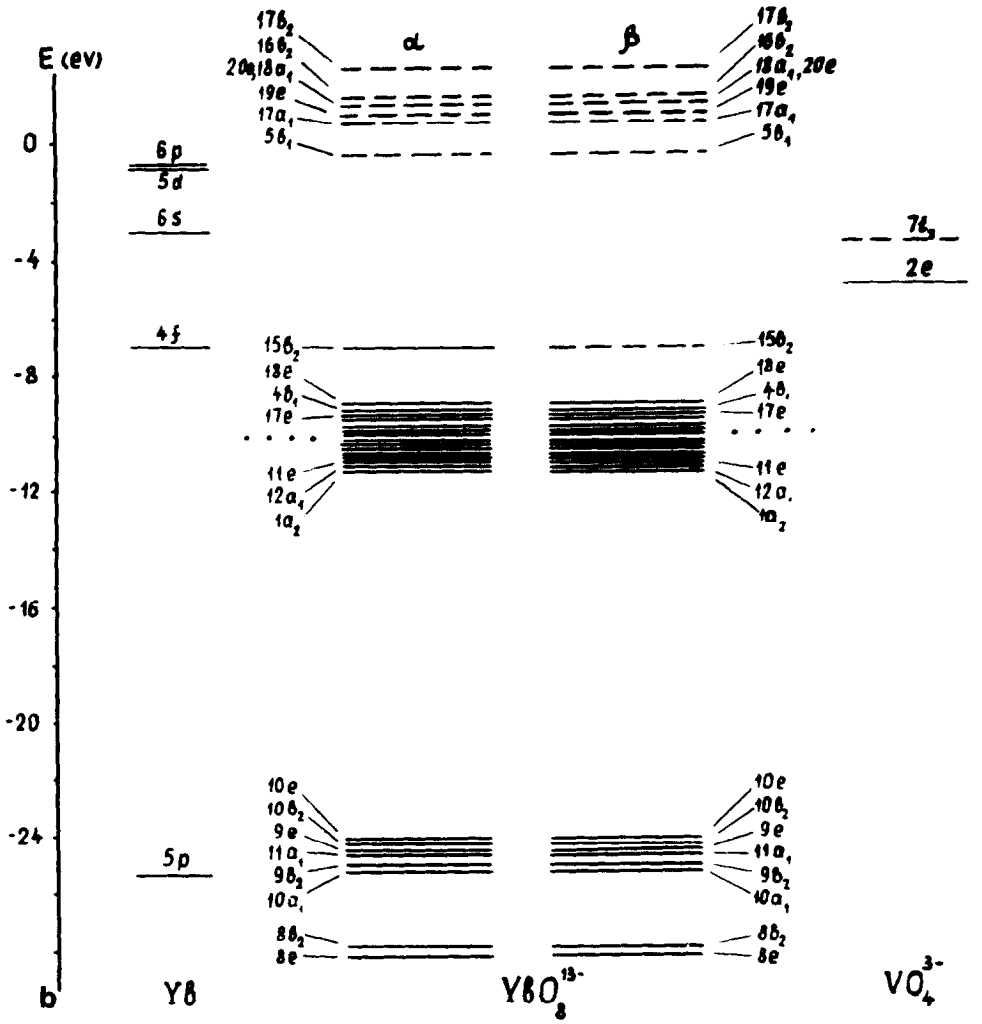

FIG. 5—*Continued*

Let us first consider the optical spectrum of the experimentally well-studied yttrium orthovanadate, which is isostructural to the *R*OVs but possesses no occupied 4*f* electrons.

In the diffuse reflection spectra of all vanadates of type RVO_4 (*7*) there appear to be two broad bands at energies ~3.9 and ~4.8 eV. The relatively weak influence of the cation *R* on these spectral characteristics leads to the assumption that the absorption is caused by the $(VO_4)^{3-}$ centers. The excitation spectra (*29*) provide an analogous picture for this range of energy. In addition, quite well-resolved transitions at 6.0 and 8.5 eV are observed which are less well understood. From Fig. 2a, it follows that the most intense excitation bands (and corresponding bands in the absorption spectra) at 3.9 and 4.8 eV can be justifiably assigned to the transitions $1t_1 \rightarrow 2e$ and $6t_2 \rightarrow 2e$ of the $(VO_4)^{3-}$ center. The considerable width of the bands is doubtless due to overlapping transitions arising from the distorted tetrahedral structure of $(VO_4)^{3-}$ in the vanadate lattice. Splittings of the relevant $1t_1$, $6t_2$, and $2e$ levels are evident in the distorted cluster results given in the second column of Fig. 2a. Similar conclusions can be

TABLE II

SPIN-POLARIZED ORBITAL ENERGIES (Rydberg) FOR THE $(EuO_8)^{13-}$ CLUSTER

Orbital	Energy		Orbital	Energy	
	Spin ↑	Spin ↓		Spin ↑	Spin ↓
$1a_1$ (Eu $1s$)	−3349.39	−3349.39	$1a_2$	−0.856	−0.750
$2a_1$ ($2s$)	−532.33	−532.32	$12e$	−0.838	−0.762
$1e$ ($2p$)	−506.35	−506.34	$11b_2$	−0.834	−0.827
$1b_2$			$13a_1$, $13e$	−0.828	−0.802
$3a_1$ ($3s$)	−117.03	−116.77	$3b_1$	−0.812	−0.808
$2b_2$ ($3p$)	−105.46	−105.23	$14a_1$	−0.809	−0.775
$2e$			$12b_2$	−0.794	−0.783
$1b_1$ ($3d$)	−83.73	−83.55	$13b_2$	−0.765	−0.756
$3b_2$, $3e$, $4a_1$			$14e$	−0.763	−0.739
$4e$ (0 $1s$)	−37.87	−37.87	$15a_1$	−0.747	−0.721
$4b_2$, $5a_1$, $5e$			$2a_2$	−0.745	−0.720
$5b_2$, $6a_1$			$15e$	−0.732	−0.717
$7a_1$ (Eu $4s$)	−23.06	−22.56	$16a_1$	−0.722	−0.392
$6b_2$ ($4p$)	−18.56	−18.06	$16e$	−0.718	−0.676[a]
$6e$			$3a_2$	−0.718	−0.410
$2b_1$ ($4d$)	−10.52	−10.03	$17e$	−0.716	−0.394
$7b_2$, $7e$, $8a_1$			$14b_2$	−0.714	−0.710
$9a_1$ ($5s$)	−3.080	−2.838	$4b_1$	−0.711	−0.711
$8e$ ($5p$)	−1.983	−1.916	$18e$	−0.676[a]	−0.379
$8b_2$	−1.957	−1.887	$15b_2$	−0.664	−0.240
$10a_1$	−1.856	−1.854	$5b_1$	−0.128	−0.057
$9b_2$	−1.856	−1.854	$19e$	−0.036	+0.035
$11a_1$	−1.829	−1.828	$17a_1$	−0.005	+0.064
$9e$	−1.811	−1.210	$18a_1$	+0.054	+0.083
$10b_2$	−1.741	−1.616	$20e$	+0.070	−0.075
$10e$	−1.730	−1.605	$16b_2$	+0.083	+0.089
$12a_1$	−0.861	−0.824	$17b_2$	+0.110	+0.189
$11e$	−0.857	−0.814			

[a] Last occupied levels.

drawn from results of self-consistent MS–$X\alpha$ calculations on $(VO_4)^{3-}$ (*22*) and calculations based on the CNDO-configuration interaction scheme (*30*). According to the results of the MS method, the energies of the $1t_1 \rightarrow 2e$ and $6t_2 \rightarrow 2e$ transitions are 4.2 and 4.8 eV, respectively; in the present work they are 5.2 and 6.0 eV, and from Ref. (*30*) a broad band from 3.3 to 3.8, 4.8, and 6.0 eV. Assignment of the 4.8-eV line to transitions connected with Y–O charge transfer (*31*), or other excitation processes as suggested in (*32*), can hardly be correct.

The transition, $2e \rightarrow t_1$, which corresponds to the molecular transition $^1T_2 \rightarrow {}^1A_4$, with an accompanying Stokes shift of 130 nm is responsible, as supposed by Shul'gin *et al.* (*7*), for the wide band at 2.76 eV (see Fig. 6a) in the luminescence spectrum of YVO_4. The nature of the other two, less-intense bands in the excitation spectra is somewhat less defined. The $(VO_4)^{3-}$ transitions $5t_2 \rightarrow 2e$ and $t_1 \rightarrow 7t_2$ contribute to the band at energy 6.0 eV, with energies calculated by the various methods as: MS–$X\alpha$, 5.8 and 5.4 eV (*22*); the present DV–Xα, 7.0 and 6.6 eV; CNDO-configuration interactions, 6.0 eV (*30*). Moreover, in the same energy region charge transfer transitions appear within the $(YO_8)^{13-}$ cluster (Fig. 2b). The excitation band at 8.5 eV is apparently

TABLE III

RARE EARTH ATOMIC ORBITAL CHARGE AND SPIN DENSITIES (MULLIKEN POPULATIONS) FOR $(RO_8)^{13-}$ CLUSTERS

	Atomic Orbital[a]					
Cluster	4*f*	5*s*	5*p*	5*d*	6*s*	6*p*
CeO_8^{13-}	1.187	0.998	2.994	0.496	0.018	0.027
	0.131	0.999	2.996	0.493	0.016	0.024
	1.318	1.997	5.990	0.989	0.034	0.051
	1.056	−0.001	−0.002	0.003	0.002	0.003
NdO_8^{13-}	3.330	0.998	2.995	0.505	0.022	0.030
	0.127	0.999	2.998	0.552	0.018	0.024
	3.457	1.997	5.993	1.057	0.040	0.054
	3.203	−0.001	−0.003	−0.047	0.004	0.006
EuO_8^{13-}	6.109	0.998	2.995	0.539	0.023	0.031
	0.125	1.000	3.000	0.457	0.017	0.023
	6.234	1.998	5.995	0.996	0.040	0.054
	5.984	−0.002	−0.005	0.082	0.006	0.008
GdO_8^{13-}	6.997	0.998	2.994	0.506	0.028	0.034
	0.143	1.000	3.000	0.439	0.023	0.027
	7.140	1.998	5.994	0.945	0.051	0.061
	6.854	−0.002	−0.006	0.067	0.005	0.007
TbO_8^{13-}	6.997	0.998	2.995	0.499	0.028	0.033
	1.197	1.000	3.000	0.447	0.024	0.028
	8.194	1.998	5.995	0.946	0.052	0.061
	5.800	−0.002	−0.005	0.052	0.004	0.005
DyO_8^{13-}	6.997	0.998	2.995	0.494	0.029	0.033
	2.269	1.000	3.000	0.453	0.025	0.029
	9.266	1.998	5.995	0.947	0.054	0.062
	4.728	−0.002	−0.005	0.041	0.004	0.004
YbO_8^{13-}	6.997	0.999	2.997	0.438	0.032	0.034
	6.013	0.999	3.000	0.436	0.032	0.034
	13.010	1.998	5.997	0.874	0.064	0.068
	0.984	0.0	−0.003	0.002	0.0	0.0
YO_8^{13-}		[Kr]	$4d^{1.101}$	$5s^{0.089}$	$5p^{0.101}$	

[a] First row—atomic orbital population for spin ↑ electrons. Second row—population for spin ↓ electrons. Third row—electron configuration, ↑ + ↓ (1*s* ··· 4*d* orbitals fully occupied). Fourth row—spin density, ↑ − ↓.

completely due to transitions from higher occupied orbitals of the oxygen 2*p* band into vacant *d*-type MO's of $(YO_8)^{13-}$. This conclusion is also confirmed by the semiempirical calculations, which made use of 75 excited configurations, and show a complete absence of transitions in the range 6–9 eV which could be connected with $(VO_4)^{3-}$ in the yttrium orthovanadate.

Substitution of a rare-earth ion with a partially occupied 4*f* shell for yttrium in RVO_4 obviously leads to a more complex level structure, as seen previously from the level diagrams of Figs. 2–5. This complexity is im-

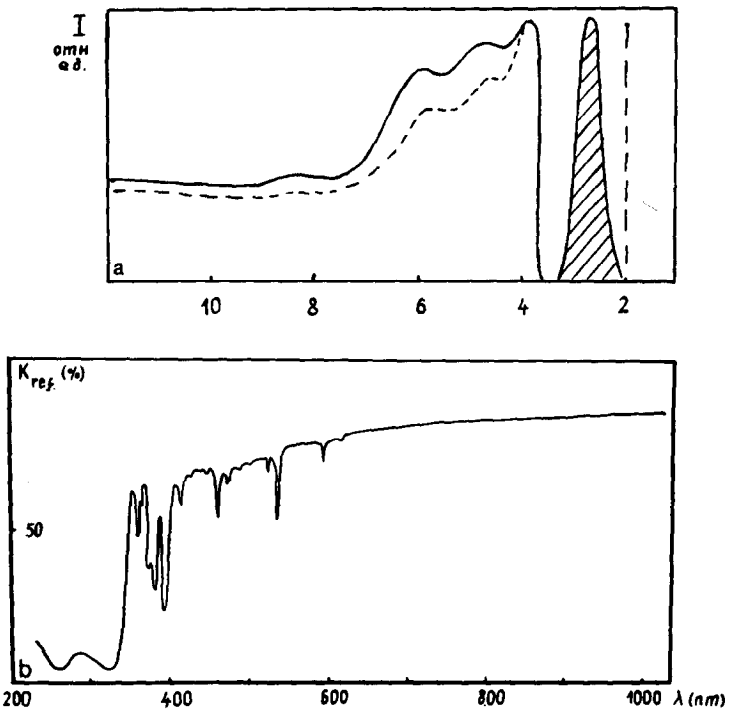

FIG. 6. Experimental spectra: (a) solid line: excitation spectra of YVO_4; dashed line: YVO_4–Eu, showing the self-luminescence spectrum of YVO_4, and the position of the most intense luminescent band of europium; (b) diffuse reflection spectrum of $EuVO_4$.

mediately reflected in the intensively studied absorption, reflection, excitation, and luminescence spectra of the *R*OV compounds, a review of which is given in Ref. (*7*). Nevertheless, quite a large number of questions remain about the nature of the optical characteristics, especially luminescence processes and mechanisms of energy transfer between excited $(VO_4)^{3-}$ groups and the rare-earth ions. The MO level structures calculated in the present work provide semiquantitative answers to some of these questions.

Similar to yttrium orthovanadate, the diffuse reflection spectra (and excitation spectra) of *R*OVs have broad bands of energy 4.7–4.9 and 3.7–3.9 eV. Also, the luminescence spectra show a broad band at ~450 nm, the intensity of which is critically dependent upon concentration of the luminescent rare-earth ion and temperature (*32*). For example, the introduction of 0.5% europium almost completely extinguishes this luminescent band (*6*). The reflection bands, as in the case of YVO_4, clearly are due to electron transitions within the distorted $(VO_4)^{3-}$ tetrahedron. Some very small and difficult to detect band shifts characteristic of $(VO_4)^{3-}$, are seen and are connected with small changes of the tetrahedral geometry within the crystal lattice of different vanadates (*10–13*).

The introduction of rare-earth ions into this lattice leads usually to the appearance of complicated systems of narrow bands in the reflection spectra, excitation spectra (excluding Gd from a number of the compounds calculated here), and luminescence (except Tb). Such lines, of course, are connected with transitions of the $4f$ electrons. As a rule, except for differences in line intensity, the spectra are very similar for a given rare-earth vanadate, and for YVO_4 (or $GdVO_4$) which may be activated by the rare-earth ion (*7*).

The luminescence of the $(VO_4)^{3-}$ ion, and the decrease in lifetime of excited states observed experimentally (*6*) indicates the presence of an energy transfer mechanism from

the vanadate group to the rare-earth ion. In the best-known compound of this type, YVO_4–Eu, emission from the $(VO_4)^{3-}$ ion is not usually observed but with excitation at the appropriate wave length (corresponding to transitions to the $2e$ MO) very strong Eu luminescence is seen. The spectra are found in the interval 1.7–2.5 eV, with the most intense line at 2.0 eV (see Ref. (*32*) and Fig. 6). The effective energy transfer can be inferred by comparing the MO energies and eigenvectors of $(VO_4)^{3-}$ and $(EuO_8)^{13-}$ clusters. The excited vanadate $2e$ orbital not only contains V–$3d$ character, but also quite an essential O–$2p$ contribution, and falls at practically the same energy as vacant "$4f\downarrow$" states of the $(EuO_8)^{13-}$ cluster (see Fig 2c). These "$4f\downarrow$" states also contain significant O–$2p$ character and it is obvious from Fig. 1 that the shared oxygen character provides an excitation channel once the necessary resonance energy condition is established. The deexcitation of these $4f\downarrow$ states takes place by spin-forbidden transitions to the $15b_2\uparrow$ orbital (Fig. 2c) which is again of predominantly $4f$ character, and leads to the appearance of narrow luminescent bands of Eu in the orthovanadate lattice.

From Fig. 2, it also appears that conditions for resonant energy transfer $(VO_4)^{3-} \rightarrow (EuO_8)^{13-}$ are also satisfied for excitations to the $7t_2$ vanadate level. This transition corresponds to the second, less intense, band in the vanadate excitation spectra (Fig. 6a). Experiments show that Eu really does luminesce under excitation of the $7t_2$ level (*32*). In principle, it is also possible to directly excite $4f$ MO levels of the Eu cluster with an energy of ~3.7 eV; however, this process is apparently much less effective than excitation through the vanadate ions (*7*).

The diffuse reflection spectrum of $EuVO_4$ given in Ref. (*7*) (which is analogous to that of YVO_4–Eu presented in Ref. (*32*)) shows several interesting features. Besides the characteristic $(VO_4)^{3-}$ maxima at 3.8 and 4.9 eV, there appears a complicated system of narrow lines with energies ~3.0–3.5 eV which are interpreted as Eu–Eu transitions. In the excitation spectrum around 350–500 nm, there also appear transitions which are connected with direct excitation of Eu levels (energy interval 2.7–3.4 eV). From Fig. 2c, we suggest that these transitions take place from the valence band (with O–$2p$ and Eu–$4f$ character) into the $4f\downarrow$ levels, or, less likely, of $(f \rightarrow f)$-type exciting the $15b_2\uparrow$ level. Since correlation effects among the f-electrons are important, it is not expected that $f \rightarrow f$ energies will be predicted accurately by an MO level scheme. Nevertheless, the theoretical energies of 3.6–4.0 eV (or 2.5 eV for $f\uparrow \rightarrow f\uparrow$) agree reasonably well with the experimental data.

6. Absorption Spectra and Luminescence of the Tb, Gd, Dy, Nd, Ce, and Yb Orthovanadates

While the introduction of europium in the vanadates under study gives a very efficient crystal phosphor, terbium is quite inactive (*7*, *32*). (This is in contrast to RPO_4 systems, where terbium reveals an intense green luminescence (Ref. *5*.)) Nevertheless, Tb is a very effective quencher of the $(VO_4)^{3-}$ luminescence (*6*). The diffuse reflection spectrum for terbium (Fig. 7a) is anomalous, for which f transitions in the visible range are almost absent (weak lines are found at 2.5 and 2.3 eV), with a broad band around 3.6 eV (*7*, *34*).

Several mechanisms have been put forward to explain the absence of Tb^{3+} luminescence in the vanadates. According to Refs. (*35*, *36*), the quenching mechanism is due to a charge transfer *from* Tb *to* V, in which the absorbed photon initiates an electron transfer of the type $(Tb^{3+}–O^{2-}–V^{5+}) \rightarrow (Tb^{4+}–O^{2-}–V^{4+})$. The remaining excitation energy is supposed to be dissipated over vibrational levels of the crystal. Another point of view is that the lattice is ineffective in transferring energy to the activator (*35*). According to Ref. (*36*), however, the probability of such energy transfer is high, but the radiation process of the Tb ion is, instead, ineffective.

Inspection of the energy level diagrams for $(VO_4)^{3-}$ and $(TbO_8)^{13-}$ (Fig. 4b) shows that the absence of luminescence is due to the lack of resonance conditions for energy transfer from the vanadate ion to $4f$ levels of the terbium cluster. This contrasts to the analogous $(EuO_8)^{13-}$ cluster where the groups of levels $(18e\downarrow–3a_2\downarrow)$ and $15b_2\downarrow$ of predominant Eu–$4f$ character lie quite near the $2e$ and $7t_2$ levels of

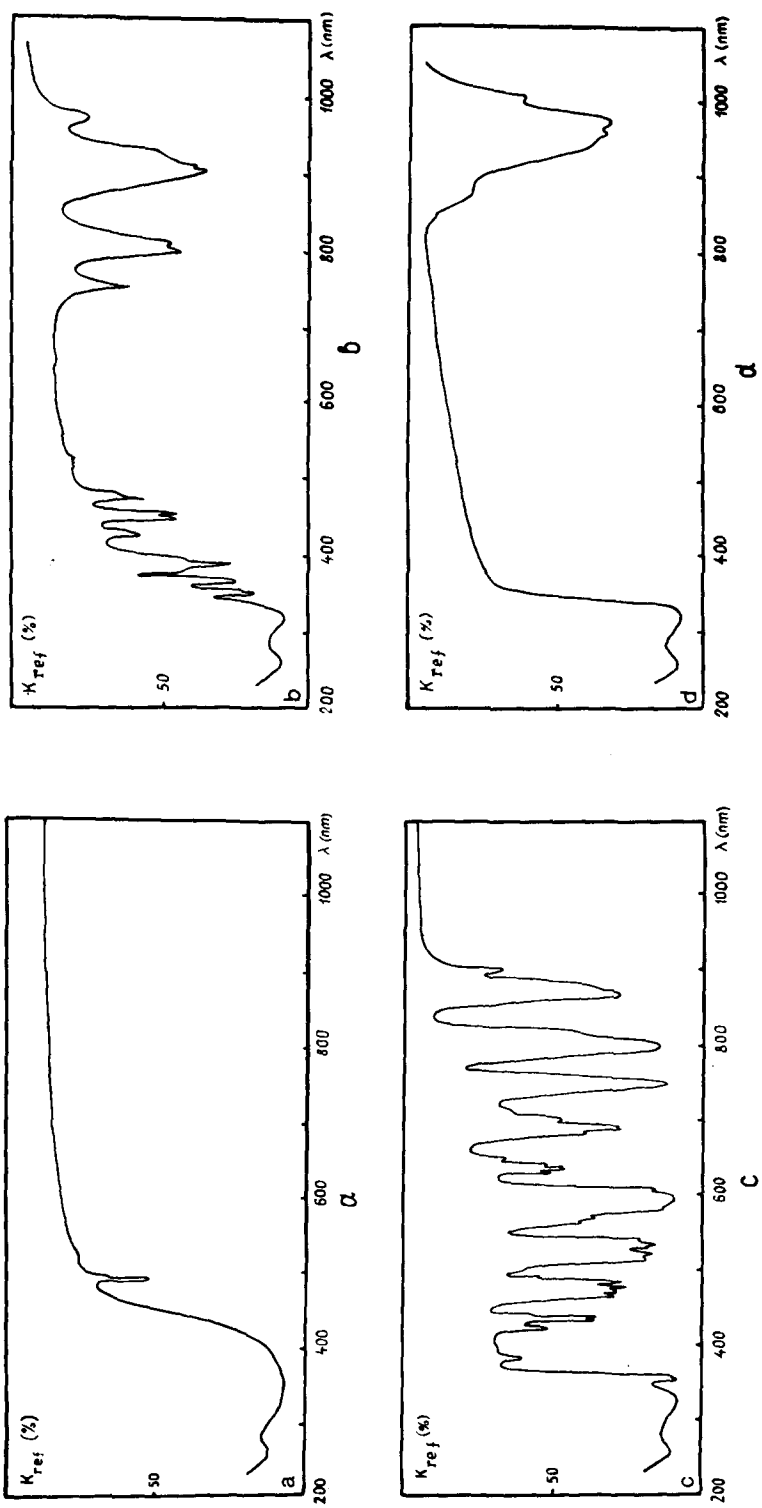

FIG. 7 Diffuse reflection spectra of (a) $TbVO_4$, (b) $DyVO_4$, (c) $NdVO_4$, (d) $YbVO_4$.

$(VO_4)^{3-}$, respectively. Comparison of the terbium and europium systems thus demonstrates the great importance of orbital energy matching for efficient energy transfer. Moreover, in the case of Tb, the low-lying spin ↑ MO's (for example, $15b_2\uparrow$) are fully occupied, so that the "$f\downarrow \rightarrow f\uparrow$" luminescence is blocked. Of course, the resonance conditions can be established by introducing relative level shifts between $(VO_4)^{3-}$ and $(TbO_8)^{13-}$ through different crystal structures, or, as in RPO_4, by replacing vanadium by a different cation.

The additional broad band seen in the diffuse reflection spectrum of $TbVO_4$ (Fig. 7a) can be interpreted as transitions from the occupied $3a_2\downarrow$ MO to the higher $15b_2\downarrow$ orbital of $4f$ type, or excitations from the O–$2p$ band to vacant $4f\downarrow$ levels. The calculated excitation energy of ~3.8 eV is close to the experimental value. The low-intensity narrow lines at 2.3 and 2.5 eV are apparently connected with f–f transitions from the $15b_2\uparrow$ orbital to vacant $18e\downarrow$–$17e\downarrow$ orbitals—the calculated energies being ~1.8–2.0 eV.

The process of quenching self-luminescence of vanadate ions upon introduction of Tb into the crystal lattice is apparently that of radiationless transitions to vacant $17e\downarrow$–$18e\downarrow$ levels of $(TbO_8)_0^{13-}$. Stokes shifts of ~130 nm, characteristic of the luminescent level of the vanadate ion, bring the $2e$ level to nearly the same energy as these $4f\downarrow$ levels of the terbium cluster. Thus, resonant energy transfer to the rare-earth ion becomes possible, but transitions in the visible and ultraviolet part of the spectrum are impossible (see Fig. 4b).

Luminescence connected with $4f$ levels of the rare-earth ion is absent in $GdVO_4$ (*7*, *32*); for this reason the gadolinium compound, like YVO_4, is often used as a matrix for the introduction of other rare-earth ions as activators. From the MO scheme of $(GdO_8)^{13-}$ (Fig. 4a), it again follows that resonance conditions between vanadate and rare-earth cluster levels are not satisfied. The $2e$ orbital of $(VO_4)^{3-}$ is located well above the group $3a_2\downarrow$–$18e\downarrow$ and moreover, vacant $4f$ levels which lie below this group are absent, in contrast to $(EuO_8)^{13-}$. Energy transfer from excitation of the $2e$ MO is thus not possible.

The low-intensity band corresponding to excitation of the $7t_2$ vanadate level suggests rather inefficient energy transfer into the $15b_2\downarrow$ orbital. These levels do appear to have sufficient energy overlap for transfer to occur, particularly when we consider the finite width of the distorted vanadate t_2 "band" (see Fig. 2a). Such a process can explain the lower intensity of the *vanadate* ion luminescence and shorter lifetime of the excited vanadate ion in $GdVO_4$ as compared to YVO_4 (see Refs. (*7*, *37*)). However, this energy transfer process (~6 eV) is not sufficiently effective to produce a noticeable Gd luminescence in $GdVO_4$. (It is also possible that there is a strong damping mechanism for the Gd^{3+} ion; Ref. (*7*).) The lack of damping of the self-luminescence of the $(VO_4)^{3-}$ group is possibly due to the Stokes shift of the luminescent level to a position below the $4f\downarrow$ MOs, which have considerably higher energies than in the terbium cluster (Fig. 4b).

Dysprosium is the second most efficient activator of luminescence (after Eu) in the orthovanadate lattice. The luminescence spectrum of Dy in the range 400–700 nm includes three multiplets (*7*, *32*). The most intense lines are located in the region 2.15–2.2 eV, less intense lines at 2.5–2.65 eV, and still weaker transitions between 1.8 and 1.9 eV. A complex level system is revealed in the diffuse reflection spectrum of $DyVO_4$ (Fig. 7b) where, along with characteristic broad bands of $(VO_4)^{3-}$ are found groups of lines with energy ~1.4–1.6, 2.5–3.0, and 3.2–3.4 eV (*7*, *34*). The excitation spectrum of YVO_4–Dy in the region of 3.1–3.4 eV also shows lines due to direct excitations of the $4f$ levels of dysprosium (*33*).

From the MO diagram of Fig. 5a, it is apparent that, as for europium, the resonance conditions for energy transfer from the $2e$ level of $(VO_4)^{3-}$ into the $15b_2\downarrow$ level of $(DyO_8)^{13-}$ is very well satisfied. The vacant $16a_1\downarrow$ and $18e\downarrow$ MOs which lie ~2.2–2.5 eV below $15b_2\downarrow$ provide the required final states for the luminescent deexcitation of that level. In contrast to the europium vanadate, such transitions are spin-allowed in the simplified nonrelativistic one-electron model. Experiment gives an analogous picture of the role of spin direction in such transitions: If for $EuVO_4$ the most intense luminescent line belongs to the

transition $^5D_0$–$^7F_2$ (*7*) where one electron changes from ↓ to ↑ spin, then for $DyVO_4$ we have the $^6F_{11/2}$–$^6H_{13/2}$ transition with no spin change. The greater efficiency of Eu as an activator may be due largely to the fact that transitions from the 2*e* vanadate MO into a considerable number, $3a_2 \cdots 18e\downarrow$, of $(EuO_8)^{13-}$ levels are possible (Fig. 2c) while in the $(DyO_8)^{13-}$ cluster, only the $15b_2\downarrow$ level is available. Narrow lines in the diffuse reflection spectrum (Fig. 7b) and excitation spectrum (*33*) of $DyVO_4$ are presumably due to $f \rightarrow f$ transitions from the occupied $3a_2\downarrow$ and $17e\downarrow$ MOs into $15b\downarrow$. The calculated energies for such transitions are 2.6–3.0 eV and 3.2 eV (see Fig. 5a). Lines seen in the interval 1.4–1.6 eV are probably also connected with "$f\downarrow \rightarrow f\downarrow$" transitions; however, the calculated transitions from 0.8–1.0 eV actually have considerable O–2*p* character due to hybridization between the oxygen valence band and 4*f* orbitals.

Experimental studies have shown luminescence in the infrared region for orthovanadates activated by Nd ions (*7*, *38*, *39*). The luminescent bands lie between 1.1 and 1.4 eV, the most intense multiplet falling at 1.17 eV. The diffuse reflection spectrum of $NdVO_4$ (see Fig. 7c) shows characteristic intensive absorption at energies of 1.4–1.7, 2.0, 2.3, 2.6, 2.9, and 3.4 eV (*7*, *34*). Inspection of the energy level diagrams for $(NdO_8)^{13-}$ given in Fig. 3b shows that both 2*e* and $7t_2$ levels of the vanadate ion are close in energy to vacant $4f\downarrow$ levels of the rare-earth cluster. Except for small differences in spacing, the spin ↓ level picture is quite similar to that of the Eu Complex. The possibility for efficient energy transfer from vanadate to rare-earth ions is evidenced by the effective quenching of the self-luminescence of $(VO_4)^{3-}$ (*34*). Transitions of the type $f \rightarrow f$ from the system $3a_2\downarrow \cdots 18e\downarrow$ into the $15b_2\uparrow$ MO occur in a manner completely analogous for the europium vanadate case discussed previously, and are likewise responsible for the Nd luminescence. Calculated energies of these spin–flip transitions of 1.2–1.7 eVare in reasonable agreement with the experiment. The large number of intense lines in the diffuse reflection spectrum of $NdVO_4$ for $\lambda > 330$ nm is connected with the rich energy structure of vacant 4*f* MO's of either spin, as follows from Fig. 3b. For transitions from the occupied $3a_2\uparrow$ and $17e\uparrow$ the calculated energies span the (1.3–1.8)-eV range; however, charge transfer transitions from O–2*p* to 4*f* levels also overlap this range. From the figure we find a confirmation of, and a strong basis for the experimental suppositions of Ref. (*39*) concerning the level structure of YVO_4–Nd, concerning the small energy differences between occupied and first vacant levels.

Experimental characterization of the optical properties of Ce and Yb in the vanadates is unfortunately not as extensive as for the other rare-earth ions. It is remarked (*32*) that similar to terbium, cerium is not active in the orthovanadate crystal lattice, emitting neither in the visual nor uv regions. In (*7*, *34*) luminescence of Ce in the ir region is mentioned.

The MO level scheme for the $(CeO_8)^{13-}$ cluster given in Fig. 3a demonstrates the possibility for energy transfer from the excited $7t_2$ vanadate level into the vacant 4*f* group $3a_2\downarrow$–$15b_2\downarrow$. Deexcitation into the vacant 4*f* levels $17e\uparrow$ to $18e\uparrow$ leads to luminescence of cerium in the ir, with calculated transition energies of~1.1–1.5 eV. Experimental evidence that the energy transfer is efficient is found in the very strong damping of vanadate-ion luminescence by introduction of Ce into the crystal lattice (*34*). In principle, the level scheme of Fig. 3a shows the possibility of luminescence at very low energy (0.1–0.3 eV) due to transitions into the $15b_2\uparrow$ level. At such low energies, excitation transfer from the 2*e* vanadate level into empty $4f\uparrow$ levels and transitions among $4f\uparrow$ are also possible. The reflection spectra of $CeVO_4$ may also include *d*–*f* transitions from $3a_2\uparrow$ to $5b_1\uparrow$ orbitals at~230 nm because of the relatively high position of 4*f* levels.

The experimental diffuse reflection spectrum of $YbVO_4$ does not support lines in the uv or visible region connected with 4*f* levels, but reveals broad bands in the ir region (*7*, *34*). Weak ir luminescence bands are found for ytterbium (*38*). The MO scheme for the $(YbO_8)^{13-}$ cluster clearly shows the absence of *f*–*f* transitions in uv and visible spectral regions. Features of the diffuse reflection spectrum (Fig. 7d) with energy~1.2 eV can be assigned as charge transfer transitions from oxygen 2*p* into the vacant $15b_2\downarrow$ orbital of 4*f*

type. The reverse transitions are possibly connected with the weak ir luminescence of Yb (*7*). However, we may not exclude the possibility of *f–f* transitions between $15b_2\uparrow$ and $15b_2\downarrow$ levels, which will certainly undergo a spin-polarization splitting when full self-consistent calculations are carried out. Inspection of Fig. 5b shows that energy transfer from $(VO_4)3^-$ *d*-levels in exciting Yb luminescence is improbable. The coincidence in energy between absorption and luminescence bands gives further evidence of the absence of this mechanism in ytterbium orthovanadate (*7*).

Conclusion

The electronic structures of molecular clusters representative of the rare-earth orthovanadates have been calculated in the Hartree–Fock–Slater model, making use of a discrete variational method. By comparison with optical reflectivity, excitation, and luminescence data, we find that the one-electron MO model provides a reasonable and consistent interpretation of the experimental results. The calculations give a quantitative picture of energy levels, the effects of covalency and charge transfer, and the importance of spin-polarization. The dominant role of resonance conditions for energy transfer between $(VO_4)^{3-}$ "metal-*d*" and $(RO_8)^{13-}$ "rare-earth *f*" levels is apparent, and observed differences in activator efficiency are thereby understood.

It should be clear that the present calculations are deficient in several respects. The HFS solutions should be iterated to self-consistency in order to obtain more precise level positions and exchange splittings, the influence of more distant neighbors should be taken into account, spin–orbit and relativistic effects should be considered, etc. Some progress has been made along these lines (see Refs. *28*, *40*). It may be possible to obtain comparable results by the more rigorous Hartree–Fock–Roothaan procedure in the near future; however, we believe that the most important advances will come from a many-electron approach, either by configuration interaction or by perturbation theory. This step is essential for understanding correlations among the open shell electrons and the resulting details of multiplet structure.

Acknowledgments

The authors are happy to acknowledge numerous stimulating discussions with Professor A. J. Freeman on various aspects of the calculations. We thank B. V. Shul'gin for considerations concerning the experimental optical data for the vanadates.

References

1. A. K. Levine and F. C. Palilla, *Appl. Phys. Lett.* **5**, 118 (1964).
2. J. R. O'Connor, *Appl. Phys. Lett.* **9**, 407 (1966).
3. J. R. O'Connor, *Trans. Met. Soc. AIME* **239**, 362 (1967).
4. J. J. Rubin and L. G. Van-Uitert, *J. Appl. Phys.* **37**, 2920 (1966).
5. R. C. Ropp, *J. Electrochem. Soc.* **115**, 841 (1968).
6. M. Ya. Kodos, B. V. Shul'gin, F. F. Gavrilov, A. A. Fotiev, and V. M. Lioznyanskii, *Zh. Prikl. Spektrosk. (J. Appl. Spectrosc., Minsk)* **16**, 1023 (1972).
7. B. V. Shul'gin, A. A. Fotiev, F. F. Gavrilov, and A. A. Moskvin, "Vanadate Crystal Phosphors" Nauka, Moscow (1976).
8. D. E. Ellis and G. S. Painter, *Phys. Rev. B* **2**, 2887 (1970).
9. F. W. Averill and D. E. Ellis, *J. Chem. Phys.* **59**, 6412 (1973).
10. V. H. Schwartz, *Z. Anorg. Allg. Chem.* **323**, 44 (1963).
11. J. A. Baglio and O. J. Sovers, *J. Solid State Chem.* **3**, 458 (1971).
12. H. Feuss and A. Kallel, *J. Solid State Chem.* **5**, **11** (1972).
13. E. Patscheke, H. Feuss, and G. Will, *Chem. Phys. Lett.* **2**, 47 (1968).
14. B. J. Baran and P. J. Aymenic, *Z. Anorg. Allg. Chem.* **383**, 220 (1971).
15. G. V. Bazuev, V. A. Kilaev, and G. N. Shveikin, *Doklady Akad. Nauk USSR* **218**, 888 (1974).
16. J. A. Baglio and G. Gashurov, *Acta Crystallogr B* **24**, 292 (1968).
17. J. C. Slater, "Quantum Theory of Molecules and Solids," Vol. 4, McGraw–Hill, New York (1974).
18. C. B. Haselgrove, *Math. Computation* **15**, 323 (1961).
19. F. Herman and S. Skillman, "Atomic Structure Calculations," Prentice–Hall, Englewood Cliffs, N.J. (1963).
20. K. Schwarz, *Phys. Rev. B* **5**, 2466 (1972).
21. K. Schwarz, *Theor. Chim. Acta* **34**, 225 (1974).
22. V. A. Gubanov, J. Weber, and J. W. D. Connolly, *J. Chem. Phys.* **63**, 1455 (1975).

23. V. A. GUBANOV, D. E. ELLIS, AND A. J. FREEMAN, *Fiz. Tverd. Tela (Sov. Phys. Solid State Phys.)*, **19**, 409 (1977).
24. J. H. HERBST, D. V. LOWY, AND R. E. WATSON, *Phys. Rev. B* **6**, 1913 (1972).
25. C. BONNELLE, R. C. KARNATAK, AND C. K. JORGENSEN, *Chem. Phys. Lett.* **14**, 145 (1972).
26. R. N. PLETNEV, V. N. LISSON, V. A. GUBANOV, AND A. K. CHIRKOV, *Fiz. Tverd. Tela (Sov. Phys. Solid State Phys.)* **16**, 289 (1974).
27. V. A. PONKOV, A. A. SIDEROV, AND V. A. GUBANOV, Proc. Chem. Inst. Ural Science Center, Academy of Sciences, USSR **35**, in press.
28. J. W. D. CONNOLLY, "Approximate Methods," Modern Theoretical Chemistry, Vol. 4, Plenum Press (1976).
29. B. V. SHUL'GIN, V. YU. KARA-USHANOV, V. A. GUBANOV, E. R. IL'MAS, AND F. F. GAVRILOV, *Zh. Priklad. Spektrosk.* **23**, 332 (1975).
30. N. K. LAZUKOVA AND V. A. GUBANOV, *Zh. Strukt. Khim. (J. Struct. Chem.)*, in press.
31. R. C. ROPP, *J. Opt. Soc. Amer.* **57**, 1210 (1967).
32. R. C. ROPP, *J. Electrochem. Soc.* **115**, 940 (1968).
33. G. S. PALILLA, A. K. LEVINE, AND M. RINKEVICS, *J. Electrochem. Soc.* **112**, 776 (1965).
34. M. YA. KODOS, Ph. D. thesis, UPI, Sverdlovsk (1973).
35. G. BLASSE AND A. BRILL, *Philips Res. Rept.* **22**, 481 (1967).
36. R. G. LELESH, T. Y. TICH, B. F. GIBBSONS, P. J. ZACHIANIDIS, AND H. L. STADLER, *J. Chem. Phys.* **53**, 681 (1970).
37. B. V. SHUL'GIN, M. YA. KODOS, F. F. GAVRILOV, A. A. FOTIEV, AND G. F. SHALYANIN, *Zh. Priklad. Spektrosk.* **15**, 864 (1971).
38. N. S. POLUYECTOV AND S. A. GAVA, *Zh. Priklad. Spektrosk.* **9**, 268 (1968).
39. A. N. KAMINSKY, V. A. BOGOMOLOV, AND L. LI, *Neorg. Mater.* **5**, 673 (1969).
40. A. ROSÉN AND D. E. ELLIS, *J. Chem. Phys.* **62**, 3039 (1975).